Supporting Information

Multi-generation production of secondary organic aerosol from toluene photooxidation

Yixin Li[1], Jiayun Zhao[1], Yuan Wang[2], John H. Seinfeld[3], and Renyi Zhang[1,4*]

[1]Department of Chemistry, Texas A&M University, College Station, TX 77843, USA

[2]Division of Geological and Planetary Sciences, California Institute of Technology, Pasadena, CA 91125, USA

[3]Division of Chemistry and Chemical Engineering, California Institute of Technology, Pasadena, CA 91125, USA

[4]Department of Atmospheric Sciences, Texas A&M University, College Station, TX 77843, USA

Number of pages: 28
Number of tables: 9
Number of figures: 11

Contents

List of Figures

List of Tables

Methods

We performed experiments to evaluate the contribution of multi-generation oxidation of toluene initiated by OH radicals to SOA and BrC formation in an environmental chamber. Monodispersed seed particles consisting of $(NH_4)_2SO_4$, NH_4HSO_4, and NaCl were prepared to represent distinct particle acidity and interfacial electric fields and exposed to the oxidation products from OH-toluene reactions. The experiments of toluene oxidation were performed similarly as in our previous studies.[1] Commercially available gaseous NH_3 (2000 ppm NH_3 in N_2, Coastal Welding Supply Beaumont Texas) was injected into the chamber with a flow of 100 standard cubic centimeters per minute (sccm) for 2 min. 600 μL H_2O_2 (35 wt%, Sigma-Aldrich) and 30 μL toluene (99.5%, Sigma-Aldrich) were injected into a glass reservoir, which was then flushed into the chamber by a 10 slpm flow from a pure air generator (Aadco 737-11, Aadco Inc.) for 10 min. The gases were then mixed by a fan inside the chamber. Once desired concentrations were established, the black light lamps were turned on to initiate H_2O_2 photolysis to generate OH radicals.

Aerosols were produced by a constant output atomizer (Model 3076, TSI), dried to RH of 2% by a Nafion drier (PD-070−18T-12SS, Perma Pure), charged by a ^{210}Po bipolar charger, and analyzed by an integrated aerosol analytical system. A scanning mobility particle sizer (SMPS) consisting of a differential mobility analyzer (DMA, Model 3081, TSI) and condensation particle counter (CPC, Model 3760A, TSI) was used to select the initial particle size (100 nm) and to continuously measure the particle size growth factor, $GF = D_p/D_{0,}$ where D_p is the diameter after exposure and D_o = 100 nm is the initial diameter. The initial particle concentration was maintained at 1.5×10^4 cm^{-3}, which was measured by the CPC. An Aerosol Particle Mass Analyzer (APM, Model 3600, Kanomax) was used to measure the particle density throughout the experiments. The density for the SOA materials (ρ_{SOA}) is calculated by,

$$\rho_{SOA} = \frac{\rho GF^3 - \rho_0}{GF^3 - 1}$$

where ρ and GF are measured particle density (g cm^{-3}) and growth factor at t (min), respectively. ρ_0 is the density of $(NH_4)_2SO_4$ (1.77 g cm^{-3}), NH_4HSO_4 (1.78 g cm^{-3}), or NaCl (2.16 g cm^{-3}). The uncertainty in the density measurements was estimated to be ± 0.03 g cm^{-3}.

To measure the optical properties of exposed particles, a 1-slpm flow from the chamber was diluted by 4-slpm N_2 and introduced into a commercial integrating nephelometer (TSI 3563) and a home-built cavity ring-down spectrometer (CRDS) after 1.5 h of exposure. Light scattering (b_{sca}) and extinction (b_{ext}) at 532 nm were determined by the nephelometer and CRDS, respectively.[2] The nephelometer was calibrated by comparing measured b_{sca} with b_{ext} from CRDS when measuring ammonium sulfate particles with diameters of 100 nm, 150 nm, 200 nm, 250 nm, and 300 nm. The absorption coefficient (b_{abs}) was determined from ($b_{ext} - b_{sca}$), and the single scattering albedo (*SSA*) was calculated from b_{sca}/b_{ext}.

An ion drift - chemical ionization mass spectrometer (ID-CIMS)[44] using the hydronium reagent ion (H_3O^+) was employed to analyze gaseous concentrations with a sample flow rate of 0.5 slpm from the chamber. The sample line was heated to 70℃ to reduce wall loss. Gas-phase concentrations from toluene oxidation (i.e., toluene and oxidation products) were quantified by ID-CIMS.[3] Briefly, the concentration of species A is determined by,

$$[\mathrm{A}] = \frac{S_\mathrm{A}}{k_{PTR}\Delta t S_{RI}}$$

where S_A and S_{RI} are the mass spectrum intensities for A and reagent ions, respectively. k_PTR is the proton-transfer rate constant between A and H_3O^+.[4] $\Delta t = \frac{l}{U_i}$ is the retention time of ions, which is determined by the length of the drift tube l = 8 cm and the ion drift velocity U_i. The ion drift velocity U_i is determined from:

$$U_i = u_0(\frac{760\ torr}{p})(\frac{T}{273\ \mathrm{K}})E$$

where u_0 = 2 cm^2 V^{-1} s^{-1} is the reduced ionic mobility[5], p = 5.0 torr, T = 298 K, and E = 37.5 V cm^{-1} is the voltage gradient in the drift tube. Alternatively, the concentrations of toluene, glyoxal, and methylglyoxal were also calibrated by preparing their vapors with known mixing ratios in N_2.[6] In our CIMS configuration, formation of cluster ions was effectively suppressed, since a uniform electrical field in the drift tube decomposed weakly-bonded cluster ions. The detection limit (defined as 3 times of the ratio of signal to noise) for the oxidation products from toluene-OH reactions was estimated to be on the order of 50 ppt by the ID-CIMS.

In our experiments, the OH concentration, [OH], was estimated using two methods. First, we considered the steady state from the reactions,

$$\mathrm{H_2O_2} \xrightarrow{J} 2\mathrm{OH}$$

$$\mathrm{Toluene} + \mathrm{OH} \xrightarrow{k_1} \mathrm{G1}$$

where J = 3.3 × 10^{-5} s^{-1} is the photolysis rate for H_2O_2,[6] and k_1 = 5.5 × 10^{-12} cm^3 molecule^{-1} s^{-1} is reaction rate between OH and toluene.[7] The steady-state OH concentration is expressed by,

$$[\mathrm{OH}]_\mathrm{ss} = \frac{J[\mathrm{H_2O_2}]}{k_1[\mathrm{Toluene}]}$$

where [H_2O_2] and [Toluene], respectively, are the average concentrations of H_2O_2 and toluene corrected for wall-loss. Alternatively, the concentration of OH was estimated from exponential fitting of the measured decay of toluene concentration, $[toluene] = [toluene]_o e^{-k_2 t}$,

$$[\mathrm{OH}] = \frac{k_2}{k_1}$$

where $[\mathrm{toluene}]_\mathrm{o}$ is the initial toluene concentration and k_2 is the fitted pseudo first-order rate constant for the toluene-OH reaction. The calculated concentrations of $[\mathrm{OH}]_\mathrm{ss}$ (3 × 10^6 molecules cm^{-3}) agreed within 90% of that derived from exponential fitting (2.7 × 10^6 molecules cm^{-3}).

While the oxidation products from OH-toluene oxidations were directly detected by ID-CIMS, we also estimated loss of vapors to the chamber wall by the first-order wall-loss coefficient k_w (s^{-1}) by considering gas-phase transport within the chamber according to Zhang *et al.*:[8]

$$k_\mathrm{w} = (\frac{A}{V})\frac{\alpha_w \bar{c}}{4+\frac{\pi}{2}\left(\frac{\alpha_w \bar{c}}{\sqrt{k_\mathrm{e} D_g}}\right)}$$

where A/V is the surface to volume ratio of the chamber (equal to $6/L$ for a square chamber with L = 1 m), α_w is the mass accommodation coefficient of vapors onto Teflon chamber walls at RH = 90%, $\bar{c} = \sqrt{\frac{8k_B T}{m}}$ is the mean thermal speed of the molecules, and k_e is the coefficient of eddy diffusion. k_e is estimated to be 0.5 from the loss rate of particles,[9]

$$k_e = \frac{(\frac{\pi L \beta_0}{12})^2}{D_b}$$

where β_0 is the fractional loss rate of particles,

$$\beta_0 = \frac{dN}{Ndt} = \frac{15000\ \text{cm}^{-3} - 7500\ \text{cm}^{-3}}{15000\ \text{cm}^{-3} \times 7200\ \text{s}} = 1.4 \times 10^{-5}\ \text{s}^{-1}$$

D_b = 6.75 × 10^{-10} m^2/s is the Brownian diffusion coefficient for particles. D_g is the gas-phase diffusion coefficient. For NH_3, the mass accommodation coefficient of vapors onto the chamber wall is 0.05.[10] Gas-phase diffusion constant D_g is 1.98 × 10^{-5} m^2 s^{-1}. The mean thermal speed $\bar{c}$ is 603 m s^{-1}. The first-order wall-loss coefficient of NH_3 is calculated to be 1.2 × 10^{-2} s^{-1}.

The average concentration of a gas species (A) is estimated by,

$$\overline{[A]} = \frac{1-e^{-k_w \Delta t_i}}{k_w \Delta t_i}[A]_0$$

For initial injection of 400 ppb NH_3, the average concentration of NH_3 was estimated to be 19 ppb. The first-order wall-loss rate of NO_x was measured to be 2.5 × 10^{-3} h^{-1}, leading to negligible wall-loss.[11]

To analyze the particle-phase chemical composition by thermal desorption - ion drift - chemical ionization mass spectrometer (TD-ID-CIMS),[12] seed particles after 20 min of exposure to photooxidation were collected for 2 hours by a platinum filament in a 2.5 slpm flow from the reaction chamber, and the analytes were evaporated by heating the filament and detected by ID-CIMS using H_3O^+ as the reagent ions.

The measured particle growth at t = 90 mins was used to derive the uptake coefficient of methylglyoxal/glyoxal from,

$$\gamma = \frac{4 \times FR \times k_1}{\bar{c} \times S}$$

where FR is the percent contributions of condensable organic species from toluene-OH oxidation to the particle-phase mass intensity (Table S2). k_1 is first-order uptake rate constant of condensable oxidized organics COO (glyoxal, methylglyoxal, γ-dicarbonyls, organic acids, and LVO), which is calculated from the measured size-growth of seed particles,

$$k_1 = \frac{\pi \times (D_p^3 - D_0^3) \times \rho \times N \times N_A}{6 \times \text{MW} \times [\text{COO}] \times \Delta t}$$

where D_p and D_0 are the final and initial diameters of the particles during the time-period of Δt = 90 min, respectively, ρ is the density of total SOA (1.6 g cm^{-3} at RH = 90% and 1.45 g cm^{-3} at RH = 10%), N = 15000 cm^{-3} is the measured particle number concentration, N_A is Avogadro constant, MW is the molar weight, and [COO] is the average gas-phase concentration. $\bar{c}$ is the mean thermal speed of A. S is the average surface-area of aerosols (cm^2 cm^{-3}) at Δt = 90 min,

$$S = \frac{\pi \int_{t=0}^{90\ \mathrm{min}} D^2 \times HGf^2 \times N \times dt}{\Delta t}$$

where D is the time-dependent diameter and HGf is the hygroscopic growth factor.[13] Results of the derived γ values are summarized in Table 1. The error bars of the uptake coefficients were estimated from the uncertainties for the parameters in Table S6 (i.e., 1 σ of at least three repeated measurements for each parameter).

References

(1) Li., Y.; Ji, Y.; Zhao, J.; Wang, Y.; Shi, Q.; Peng, J.; Wang, Y.; Wang, C.; Zhang, F.; Wang, Y.; Seinfeld, J. H.; Zhang, R. Unexpected Oligomerization of Small α-Dicarbonyls for Secondary Organic Aerosol and Brown Carbon Formation. *Environ. Sci. Technol*. **2021,** *55*, doi.org/10.1021/acs.est.0c08066.

(2) Khalizov, A. F.; Xue, H.; Wang, L.; Zheng, J.; Zhang, R. Enhanced Light Absorption and Scattering by Carbon Soot Aerosol Internally Mixed with Sulfuric Acid. *J. Phys. Chem. A* **2009**, *113* (6), 1066–1074. https://doi.org/10.1021/jp807531n.

(3) Fortner, E. C.; Zhao, J.; Zhang, R. Development of Ion Drift-Chemical Ionization Mass Spectrometry. *Anal. Chem.* **2004**, *76* (18), 5436–5440. https://doi.org/10.1021/ac0493222.

(4) Zhao, J.; Zhang, R. Proton Transfer Reaction Rate Constants between Hydronium Ion (H3O+) and Volatile Organic Compounds. *Atmos. Environ.* **2004**, *38* (14), 2177–2185. https://doi.org/https://doi.org/10.1016/j.atmosenv.2004.01.019.

(5) Dotan, I.; Albritton, D. L.; Lindinger, W.; Pahl, M. Mobilities of CO_2^+, N_2H^+, H_3O^+, $H_3O^+ \cdot H_2O$, and $H_3O^+ \cdot (H_2O)_2$ ions in N_2. *J. Chem. Phys*. **1976**, *65*, 5028-5030.

(6) Li., Y.; Ji, Y.; Zhao, J.; Wang, Y.; Shi, Q.; Peng, J.; Wang, Y.; Wang, C.; Zhang, F.; Wang, Y.; Seinfeld, J. H.; Zhang, R. Unexpected Oligomerization of Small α-Dicarbonyls for Secondary Organic Aerosol and Brown Carbon Formation. *Environ. Sci. Technol*. **2021,** *55*, doi.org/10.1021/acs.est.0c08066.

(7) Atkinson, R.; Aschmann, S. M. Rate Constants for the Gas-Phase Reactions of the OH Radical with a Series of Aromatic Hydrocarbons at 296 ± 2 K. *Int. J. Chem. Kinet.* **1989**, *21* (5), 355–365. https://doi.org/https://doi.org/10.1002/kin.550210506.

(8) Zhang, X.; Cappa, C. D.; Jathar, S. H.; McVay, R. C.; Ensberg, J. J.; Kleeman, M. J.; Seinfeld, J. H. Influence of vapor wall loss in laboratory chambers on yields of secondary organic aerosol. *Proc. Natl. Acad. Sci. U.S.A.* **2014**, *111*, 5802–5807.

(9) McMurry, P.H., Rader, D. J. Aerosol Wall Losses in Electrically Charged Chambers. *Aerosol Science and Technology*, **1985**, *4*(3), 249-268.

(10) Shi, Q.; Davidovits, P.; Jayne, J. T.; Worsnop, D. R.; Kolb, C. E. Uptake of Gas-Phase Ammonia. 1. Uptake by Aqueous Surfaces as a Function of PH. *J. Phys. Chem. A* **1999**, *103* (44), 8812–8823. https://doi.org/10.1021/jp991696p.

(11) Qi, X.; Zhu, S.; Zhu, C.; Hu, J.; Lou, S.; Xu, L.; Dong, J.; Cheng, P. Smog Chamber Study of the Effects of NOx and NH3 on the Formation of Secondary Organic Aerosols and Optical Properties from Photo-Oxidation of Toluene. *Sci. Total Environ.* **2020**, *727*, 138632. https://doi.org/https://doi.org/10.1016/j.scitotenv.2020.138632.

(12) Wang, L.; Khalizov, A. F.; Zheng, J.; Xu, W.; Ma, Y.; Lal, V.; Zhang, R. Atmospheric Nanoparticles Formed from Heterogeneous Reactions of Organics. *Nat. Geosci.* **2010**, *3* (4), 238–242. https://doi.org/10.1038/ngeo778.

(13) Seinfeld, J. H.; Pandis, S. N. *Atmospheric Chemistry and Physics: From Air Pollution to Climate Change*; John Wiley & Sons, 2016.

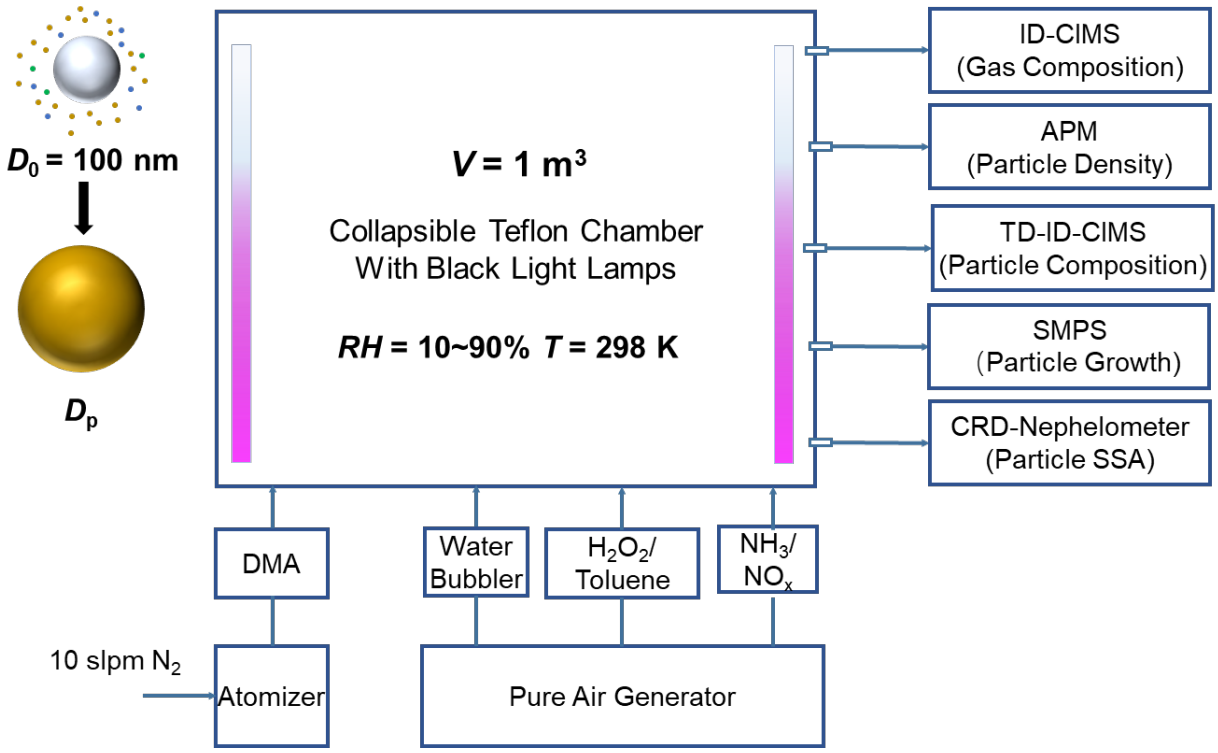

Figure S1. Schematic representation of the experimental setup. DMA for differential mobility analyzer; ID-CIMS for ion drift – chemical ionization mass spectrometry; APM for aerosol particle mass analyzer, TD-ID-CIMS for thermal desorption - ion drift – chemical ionization mass spectrometry; SMPS for scanning mobility particle sizer; and CRD for cavity ring-down spectroscopy. Monodispersed seed particles consisting of ammonium bisulfate, ammonium sulfate, and sodium chloride were exposed to oxidation products between toluene by OH and in the absence/presence of NH_3 vapors inside a 1 m^3 reaction chamber. RH was regulated between 10% and 90%, and T was maintained at 298 K. The gaseous concentrations of the oxidation products and particle properties, such as density, chemical composition, growth, and single scattering albedo, were simultaneously quantified by ID-CIMS, APM, TD-ID-CIMS, SMPS, and CRD-Nephelometer, respectively.

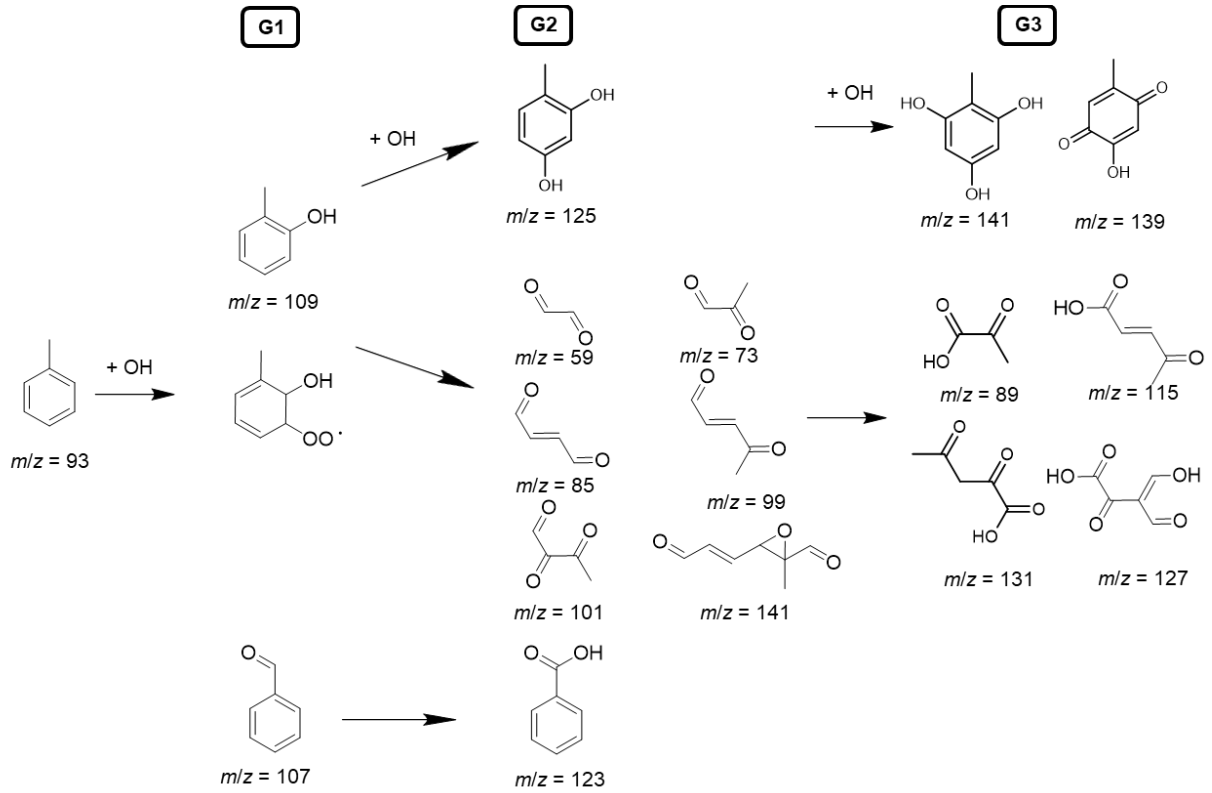

Figure S2. Multi-generation products from toluene-OH photooxidation. The letters of G1, G2, and G3 denote the sequence of reactions with OH, and the numbers denote the mass to charge ratio (*m/z*).

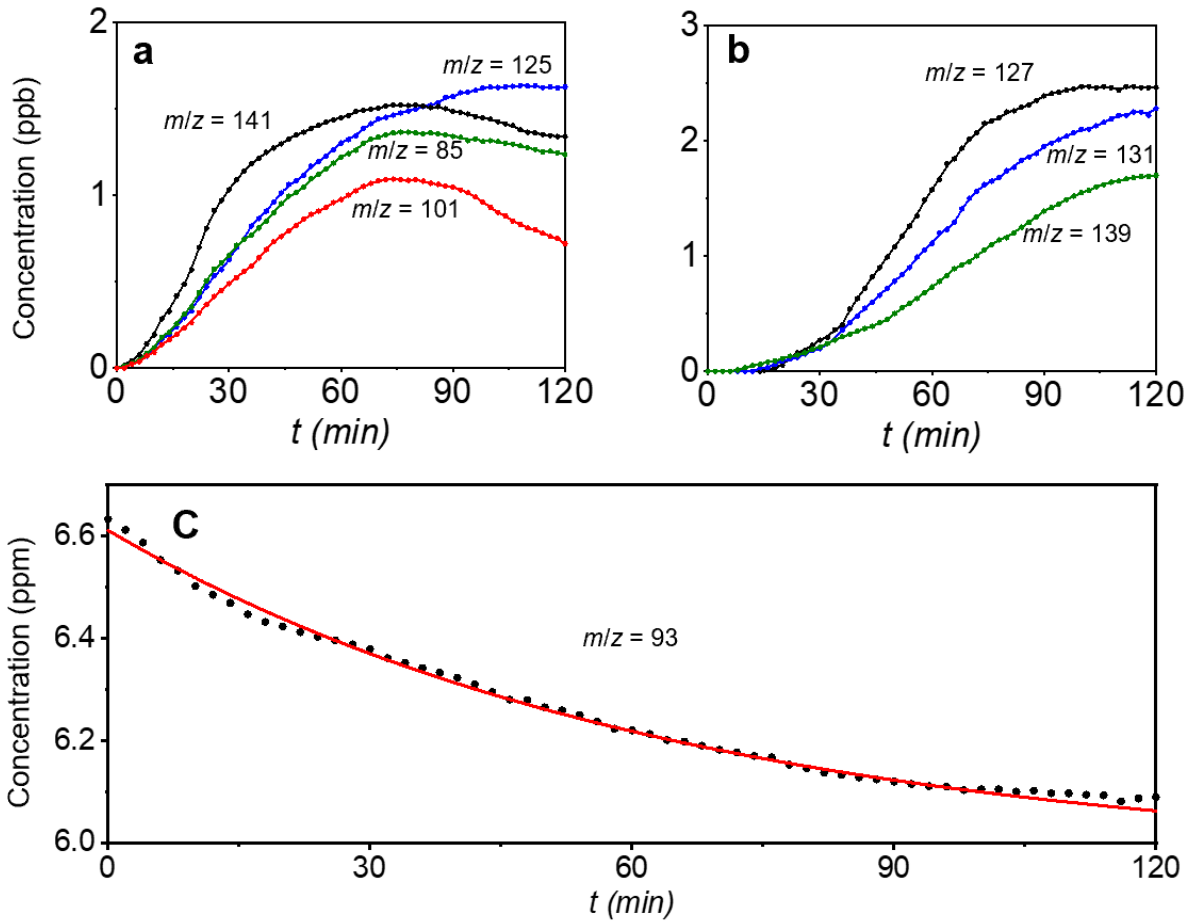

Figure S3. Temporal evolutions in products and reactants from toluene oxidation. The gaseous concentrations of G2 products (a), G3 products (b), and toluene (c). The red solid line in (c) corresponds to kinetic simulation of the toluene concentration. The initial concentration for toluene and the steady-state concentration for OH were 6.6 ppm and 2.7×10^6 molecules cm^{-3}, respectively, with a bimolecular rate constant of 5.5×10^{-12} cm^3 $molecule^{-1}$ s^{-1}. The experiments were carried out on $(NH_4)_2SO_4$ seed particles with 19 ppb NH_3 and at 298 K and RH = 90%. Initiation of photooxidation by ultraviolet light occurred at $t = 0$.

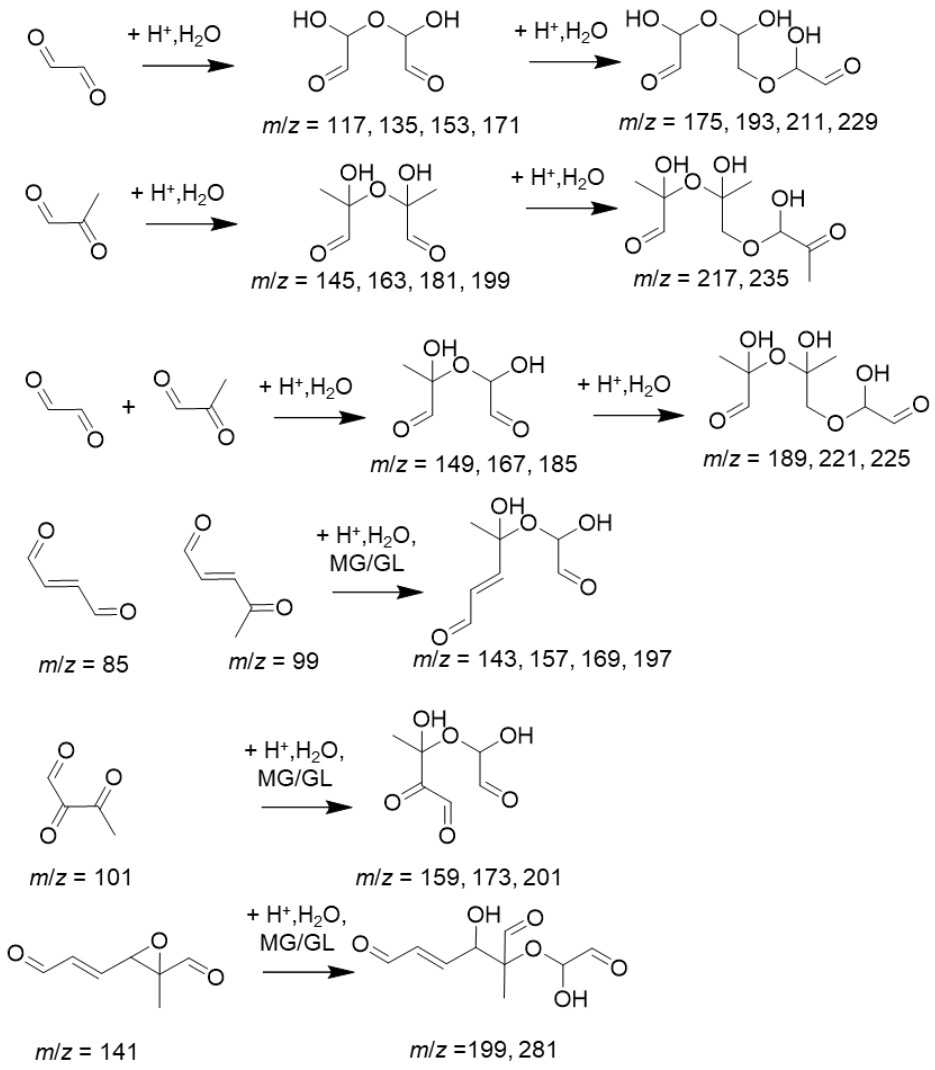

Figure S4. Pathways for oligomerization. The mechanisms leading to formation of particle-phase oligomers from α-dicarbonyls, γ-dicarbonyls, tricarbonyls, and epoxide detected by TD-ID-CIMS.

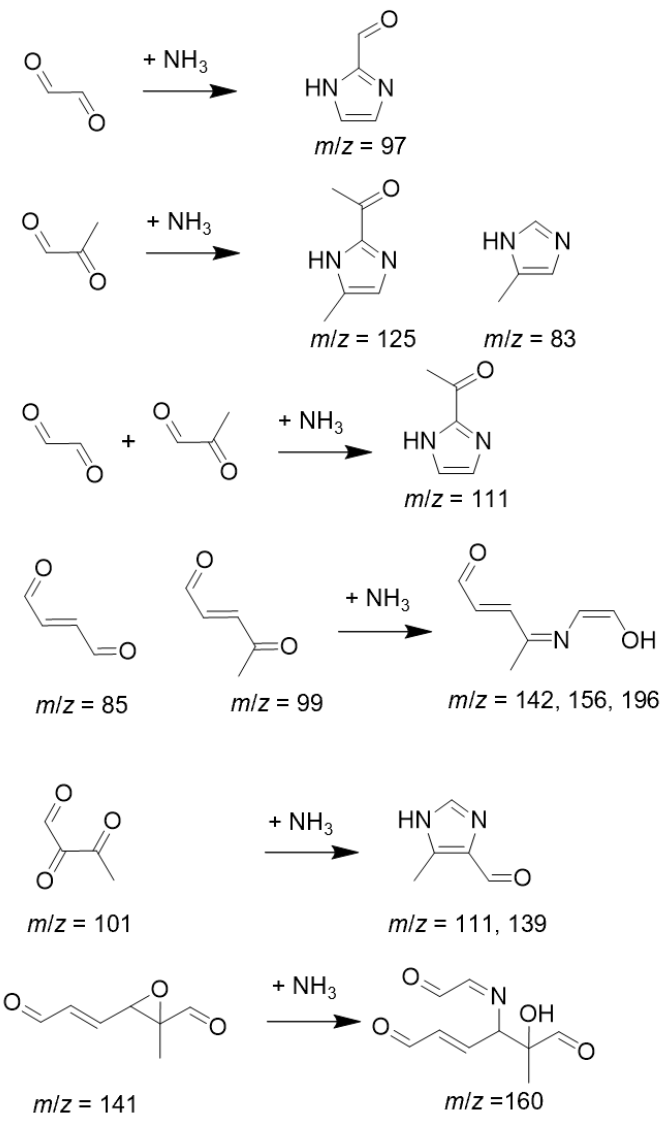

Figure S5. Pathway for BrC formation. The mechanisms leading to formation of particle-phase nitrogen-containing organics (NCO) from α-dicarbonyls, γ-dicarbonyls, tricarbonyls, and epoxide.

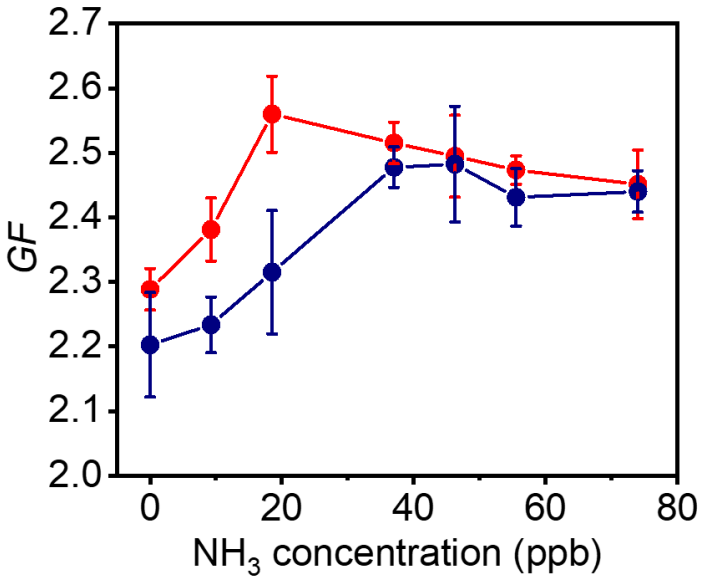

Figure S6. Size growth with NH_3. Comparison of measured *GF* at $t = 90$ mins between NH_4HSO_4 (blue) and $(NH_4)_2SO_4$ (red) seed particles exposed to toluene-OH oxidation products at varying NH_3 concentrations between 0 and 74 ppb. The error bar denotes 1σ of 3 repeated measurements. All experiments were carried out at 298 K and RH = 90%.

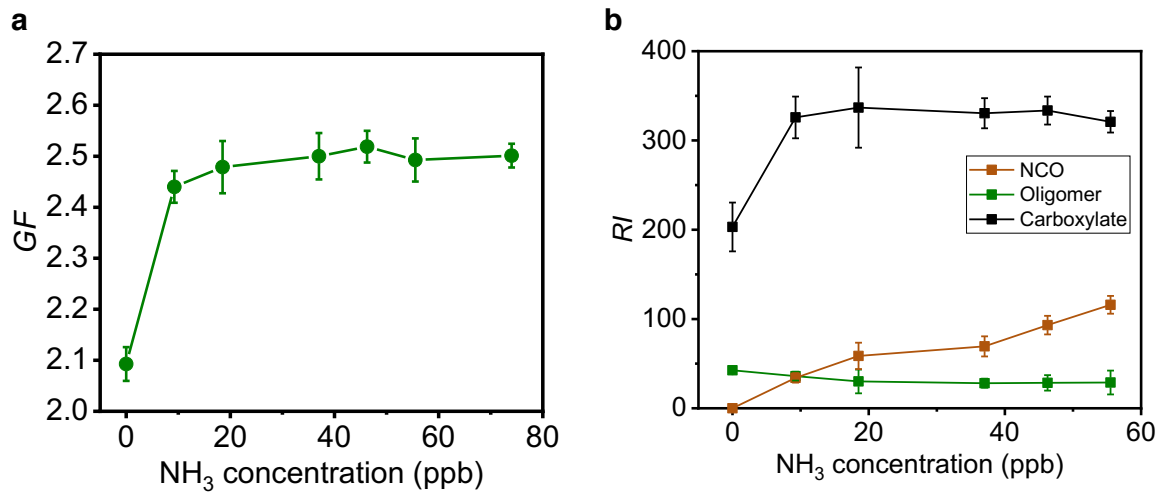

Figure S7. Variations in size growth and composition with NH_3. Measurements of *GF* and chemical compositions on NaCl seed particles exposed to toluene-OH oxidation products with varying NH_3. (a) *GF* at t = 90 mi with varying NH_3 concentrations between 0 and 74 ppb. (b) Particle-phase mass relative intensity (*RI*) for carboxylates (black), oligomers (green), and NCO (brown). The error bar denotes 1σ of 3 repeated measurements.

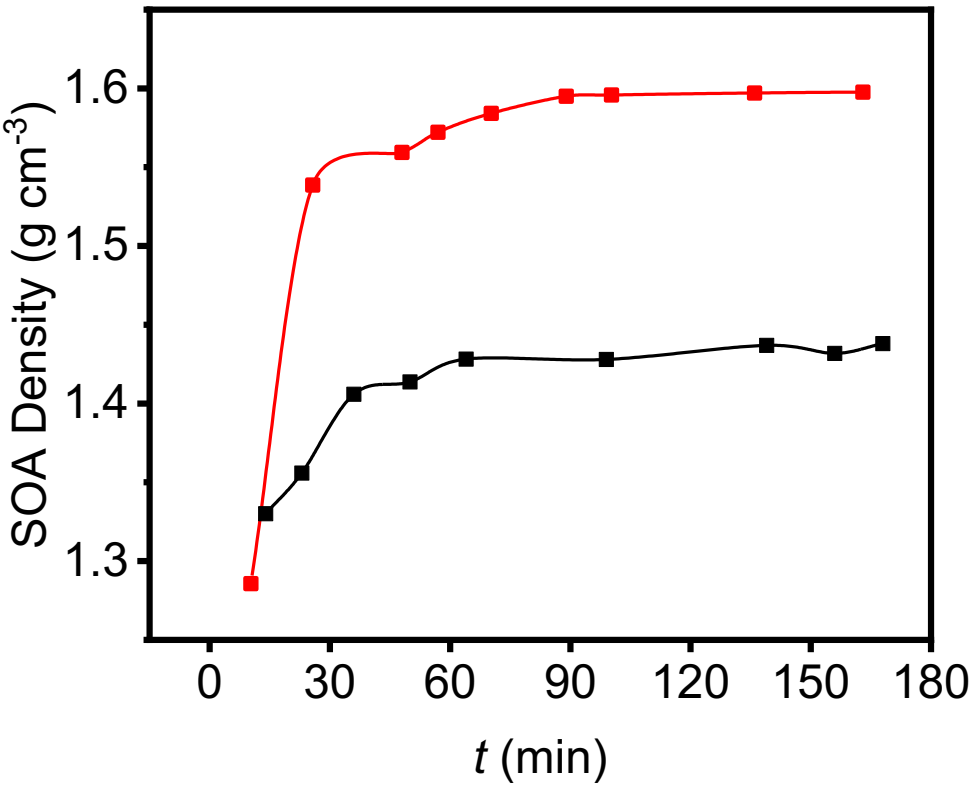

Figure S8. Temporal evolution in SOA density. SOA density at RH = 90% (red) and 10% (black). All experiments were carried out on $(NH_4)_2SO_4$ seed particles with 19 ppb NH_3. Initiation of photooxidation by ultraviolet light occurred at $t = 0$.

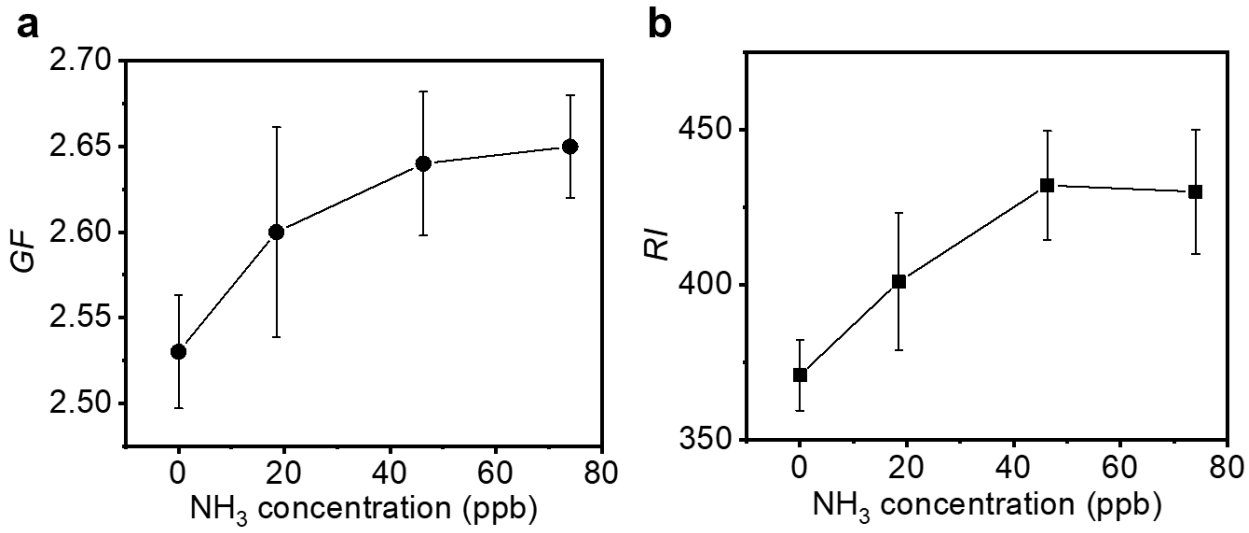

Figure S9. Variations in size growth and composition with NH_3. *GF* (a) and particle-phase mass relative intensity (*RI*) for carboxylates (b) on $(NH_4)_2SO_4$ seed particles at varying NH_3 concentrations between 0 and 74 ppb and at RH = 10%. The error bar denotes 1σ of 3 repeated measurements.

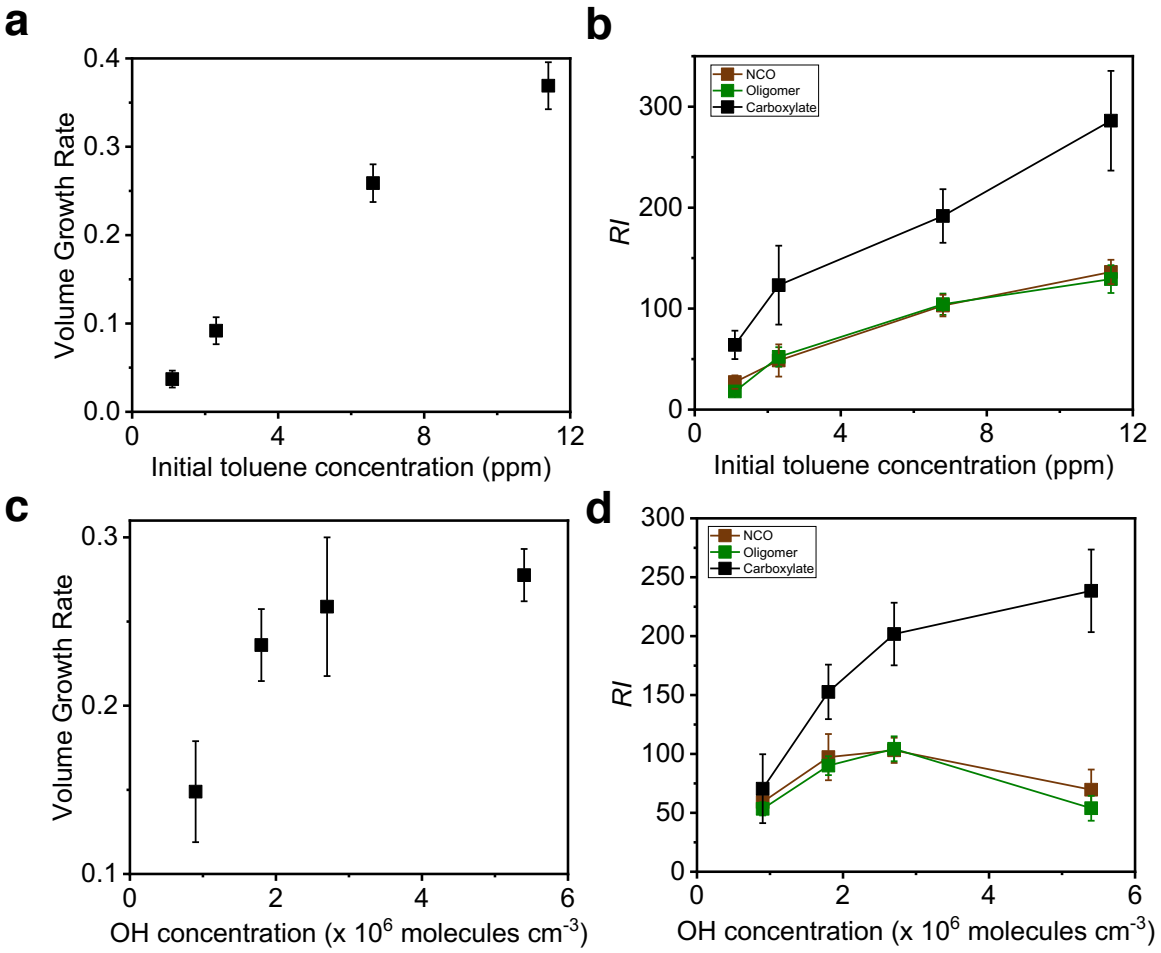

Figure S10. Variations in particle growth with reactants. Particle growth under different concentrations of toluene and OH. (a) Particle volume growth rate (defined as $GR_v = (D_2^3 - D_1^3) / (D_0^3 \Delta t)$, where D_2 and D_1, are the diameter of dry particles after 30 min and 10 min of exposure, respectively. Δt = 20 min is the time duration) with initial toluene concentration from 1.1 to 11.4 ppm. (b) Particle-phase mass intensity (*RI*) for carboxylates (black), oligomers (green), and NCO (brown) with initial toluene concentration from 1.1 to 11.4 ppm. The OH concentration in (a) and (b) is 2.7×10^6 molecules cm^{-3}. (c) Measured GR_V with OH concentration from 0.9×10^6 to 5.4×10^6 molecules cm^{-3}. (d) Particle-phase mass intensity for carboxylates (black), oligomers (green), and NCO (brown) with varying OH concentrations from 0.9×10^6 to 5.4×10^6 molecules cm^{-3}. The initial toluene concentration in (c) and (d) is 6.6 ppm. The error bar denotes 1σ of 3 repeated measurements.

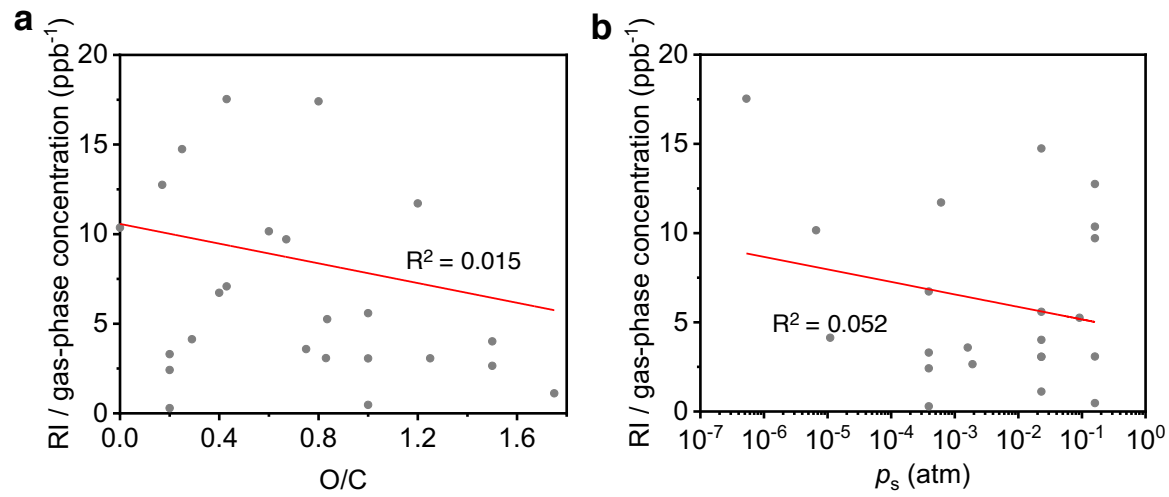

Figure S11. SOA formations versus O/C ratio and volatility. Correlation of the particle-phase mass intensity (*RI*) of identified SOA components normalized by the gaseous concentrations of the condensable oxidized organic to the oxygen-carbon (O/C) ratio (a) and the saturation vapor pressure at 298K (b). The experiments were performed on $(NH_4)_2SO_4$ seed particles with 19 ppb NH_3 at RH = 90%, similar to Figure 1h. The red solid line represents linear-fitting through the data.

Table S1. Density of identified major SOA components by TD-ID-CIMS.

Compounds	***m/z***	**Density (g cm^{-3})**
Methylimidazole	83	1.03
Methylglyoxal	73	1.05
butenedial	85	1.06
4-Oxo-2-pentenoic acid	115	1.2
Imidazole	69	1.23
Pyruvic acid	89	1.25
Benzoic acid	123	1.27
Glyoxal	59	1.27
Dihydroxy toluene	125	1.29
Acetylpyruvic acid	131	1.3
Glyoxylic acid	75	1.38
Trihydroxy toluene	141	1.4
Glyoxal oligomers	175	1.71
2-hydroxy-5-methylquinone	139	1.4
Oxalic acid	91	1.9
Methylglyoxal oligomers	127	1.9

Table S2. The percent contributions of condensable organic species from toluene-OH oxidation to the particle-phase mass intensity. GL: glyoxal, MG: methylglyoxal, GL+MG: cross-reaction of glyoxal and methylglyoxal. Note that the cross-reaction products of γ-carbonyls/tricarbonyls with α-dicarbonyls are summed into the contribution of γ-carbonyls/tricarbonyls. The experiments were carried on $(NH_4)_2SO_4$ seed particle with 19 ppb of NH_3 and with the initial concentrations of toluene and OH of 6.6 ppm and 2.7×10^6 molecules cm^{-3}, respectively.

Condensable oxidized organics	**Contribution**		
	Oligomerization	**NCO formation**	**Total**
GL	6%	7%	13%
MG	4%	6%	10%
GL+MG	6%	3%	9%
γ-dicarbonyls	5%	5%	10%
tricarbonyls	2%	4%	6%
epoxide	3%	1%	4%
Sum	26%	26%	52%
Carboxylates			40%
LVO			8%

Table S3. Mass peak assignments for nitrogen-containing organics (NCO) from α-dicarbonyls n-heterocycles and γ-carbonyls n-chains detected by TD-ID-CIMS.

m/z	MW	Formula	Compound
Methylglyoxal n-heterocycles			
83	82	$C_4H_6N_2$	
119	118	$C_4H_{10}O_2N_2$	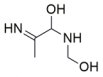
125	124	$C_6H_8ON_2$	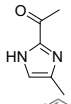
251	250	$C_6H_{10}O_5$	
Glyoxal n-heterocycles			
69	68	$C_3H_4N_2$	
97	96	$C_4H_4ON_2$	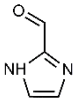
tricarbonyl n-heterocycles			
111	110	$C_5H_6ON_2$	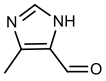
139	138	$C_6H_6O_2N_2$	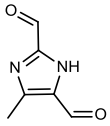
γ-carbonyls n-chains			
142	141	$C_6H_7O_2N$	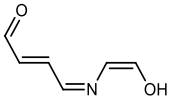
156	155	$C_7H_9O_2N$	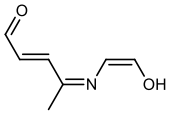
196	195	$C_4H_6O_2N_2$	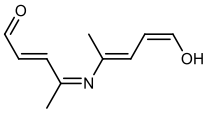

Table S4. Mass peak assignments for organic acids and low-volatile organics (LVO) detected by TD-ID-CIMS.

m/z	MW	Formula	Compound
89	88	$C_3H_4O_3$	
115	114	$C_5H_6O_3$	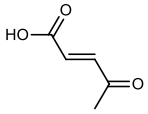
123	122	$C_7H_6O_2$	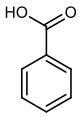
125	124	$C_7H_8O_2$	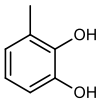
127	126	$C_5H_4O_5$	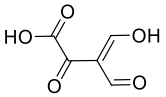
129	128	$C_6H_8O_3$	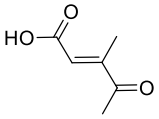
131	130	$C_5H_6O_4$	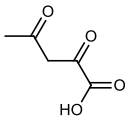
139	138	$C_7H_6O_3$	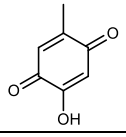

Table S5. Mass peak assignments for oligomeric products detected by TD-ID-CIMS.

	m/z	Ion	MW	Formula
Methylglyoxal				
Dimers	145	$[C_6H_{10}O_5+H-H_2O]^+$	162	$C_6H_{10}O_5$
	163	$[C_6H_{10}O_5+H]^+$	162	$C_6H_{10}O_5$
	163	$[C_6H_{12}O_6+H-H_2O]^+$	180	$C_6H_{12}O_6$
	181	$[C_6H_{12}O_6+H]^+$	180	$C_6H_{12}O_6$
	181	$[C_6H_{14}O_7+H-H_2O]^+$	198	$C_6H_{14}O_7$
	199	$[C_6H_{14}O_7+H]^+$	198	$C_6H_{14}O_7$
Trimers	217	$[C_9H_{12}O_6+H]^+$	216	$C_9H_{12}O_6$
	217	$[C_9H_{14}O_7+H-H_2O]^+$	234	$C_9H_{14}O_7$
	235	$[C_9H_{14}O_7+H]^+$	234	$C_9H_{14}O_7$
	235	$[C_9H_{16}O_8+H-H_2O]^+$	252	$C_9H_{16}O_8$
	253	$[C_9H_{16}O_8+H]^+$	252	$C_9H_{16}O_8$
	253	$[C_9H_{18}O_9+H-H_2O]^+$	270	$C_9H_{18}O_9$
	271	$[C_9H_{18}O_9+H]^+$	270	$C_9H_{18}O_9$
	271	$[C_9H_{20}O_{10}+H-H_2O]^+$	288	$C_9H_{20}O_{10}$
	289	$[C_9H_{20}O_{10}+H]^+$	288	$C_9H_{20}O_{10}$
Glyoxal				
Dimers	117	$[C_4H_6O_5+H-H_2O]^+$	134	$C_4H_6O_5$
	135	$[C_4H_6O_5+H]^+$	134	$C_4H_6O_5$
	153	$[C_4H_8O_6+H]^+$	152	$C_4H_8O_6$
	171	$[C_4H_{10}O_7+H]^+$	170	$C_4H_{10}O$
Trimers	175	$[C_6H_6O_6+H]^+$	174	$C_6H_6O_6$
	193	$[C_6H_8O_7+H]^+$	192	$C_6H_8O_7$
	211	$[C_6H_{10}O_8+H]^+$	210	$C_6H_{10}O_8$
	229	$[C_6H_{12}O_9+H]^+$	228	$C_6H_{12}O_9$
	247	$[C_6H_{14}O_{10}+H]^+$	246	$C_6H_{14}O_{10}$
tricarbonyl				
Monomers	101	$[C_4H_4O_3+H]^+$	100	$C_4H_4O_3$
	159	$[C_6H_6O_5+H]^+$	158	$C_6H_6O_5$
Dimers	173	$[C_7H_8O_5+H]^+$	172	$C_7H_8O_5$
	201	$[C_8H_8O_6+H]^+$	200	$C_8H_8O_6$
γ-dicarbonyls				
Monomers	85	$[C_4H_4O_2+H]^+$	84	$C_4H_4O_2$
	99	$[C_5H_6O_2+H]^+$	98	$C_5H_6O_2$
Dimers	143	$[C_6H_6O_4+H]^+$	142	$C_6H_6O_4$
	157	$[C_7H_8O_4+H]^+$	156	$C_7H_8O_4$
	169	$[C_8H_8O_4+H]^+$	168	$C_8H_8O_4$
	197	$[C_{10}H_{12}O_4+H]^+$	196	$C_{10}H_{12}O_4$
epoxide	141	$[C_7H_8O_3+H]^+$	140	$C_7H_8O_3$

Table S6. Measured uptake coefficient (γ) for condensable oxidized organics on ammonium sulfate seed particles in the presence of ammonia. The uncertainty in the calculated γ reflects the combined random errors in the measured five parameters, i.e., D_o = initial diameter, D_p = final diameter after the exposure time of dt, N = the particle number concentration, S = average particle surface area, and [A] = average concentration of species A. FR = percent contributions to the particle-phase mass intensity (Table S2). For each parameter, an uncertainty is estimated, corresponding to 1σ of at least 3 measurements.

Species	D_o (nm)	D_p (nm)	N (cm^{-3})	S (10^{-5} cm^2 cm^{-3})	[A] (ppb)	FR	γ (10^{-3})
RH = 90%							
Glyoxal	100.0	256.0	15000	1.55	1.9	13%	8.3 ± 2.0
Methylglyoxal	100.0	256.0	15000	1.55	0.9	10%	12 ± 2.8
γ-Dicarbonyls	100.0	256.0	15000	1.55	3.1	10%	3.0 ± 0.6
Benzoic acid	100.0	256.0	15000	1.55	0.9	0.9%	0.84 ± 0.11
4-Oxo-2-pentenoic acid	100.0	256.0	15000	1.55	1.9	4.8%	2.2 ± 0.4
Pyruvic acid	100.0	256.0	15000	1.55	0.9	2.6%	2.9 ± 0.3
LVO	100.0	256.0	15000	1.55	1.2	8.0%	5.0 ± 1.5
Nitrophenol*	100.0	246.0	15000	1.46	1.4	3.1%	1.6 ± 0.3
RH = 10%							
Glyoxal	100.0	260.0	15000	0.85	5.4	1.9%	0.75 ± 0.18
Methylglyoxal	100.0	260.0	15000	0.85	3.2	1.5%	0.90 ± 0.20
γ-Dicarbonyls	100.0	260.0	15000	0.85	9.6	2.0%	0.34 ± 0.07
Benzoic acid	100.0	260.0	15000	0.85	2.0	1.1%	0.80 ± 0.14
4-Oxo-2-pentenoic acid	100.0	260.0	15000	0.85	6.8	9.1%	2.0 ± 0.5
Pyruvic acid	100.0	260.0	15000	0.85	3.6	5.3%	2.5 ± 0.4
LVO	100.0	260.0	15000	0.85	2.9	9.4%	4.2 ± 1.5
Nitrophenol*	100.0	253.5	15000	0.82	2.3	3.0%	1.6 ± 0.3

* Measured in the presence of 100 ppb NO_x

Table S7. Relative contributions of condensable oxidized organics with each type of functionality to SOA formation on $(NH_4)_2SO_4$ seed particles with 19 ppb NH_3 and at 10% - 90% RH.

Functionality	SOA Contribution (%)			
	RH (%)			
	10	50	70	90
Di-carbonyls	3	19	22	26
Di-carbonyls+NH_3	2	14	20	26
Carboxylates	86	58	49	40
LVO	9	9	9	8

Table S8. Oxygen to carbon (O/C) ratio for identified SOA components and saturation vapor pressures (P_s) of condensable oxidized organics.

Compound	O/C	p_s (atm, 298 K)
Oligomers		
Glyoxal	1	2.3×10^{-2}
Glyoxal dimers	1~1.75	
Glyoxal trimers	1~1.67	
Methylglyoxal	0.67	1.6×10^{-1}
Methylglyoxal dimers	0.67~1.17	
Methylglyoxal trimers	0.67~1.11	
Butenedial	0.5	7.9×10^{-4}
Butenedial dimers	0.5~0.87	
Methylbutenedial	0.4	3.9×10^{-4}
Methylbutenedial dimers	0.4~0.7	
Tricarbonyl	0.75	1.6×10^{-3}
Tricarbonyl dimers	0.75~0.9	
Epoxide	0.43	
NCO		
Glyoxal N-heterocycles	0~0.25	
Methylglyoxal N-heterocycles	0~0.17	
Butenedial N-heterochains	0~0.25	
Methylbutenedial N-heterochains	0~0.2	
Tricarbonyl N-heterocycles	0.2~0.4	
Epoxide N-heterochains	0~0.44	
Organic acids		
Benzoic acid	0.29	1.1×10^{-5}
4-Oxo-2-pentenoic acid	0.6	6.6×10^{-6}
Acetylpyruvic acid	0.8	
Pyruvic acid	1.2	6.1×10^{-4}
Glyoxylic acid	1.5	1.9×10^{-3}
Others	1.25	
Dihydroxy toluene	0.29	
Trihydroxy toluene	0.43	1.1×10^{-8}
2-Hydroxy-5-methylquinone	0.43	5.3×10^{-7}

Table S9. Comparison of measured gaseous concentrations of condensable oxidized organics form toluene-OH oxidation between 10% and 90% RH.

m/z	**Average Concentration (ppb)**		**Ratio (10% to 90% RH)**
	10% RH	90% RH	
59	5.4	1.9	2.8
73	3.2	0.9	3.4
85	2.6	0.7	3.7
89	3.6	0.9	4.0
91	5.2	2.9	1.8
99	9.6	3.1	3.1
101	3.0	0.7	4.3
107	6.5	4.2	1.5
109	22.6	13.3	1.7
111	5.9	3.1	1.9
115	6.8	1.9	3.6
123	2.0	0.9	2.2
125	1.3	1	1.3
127	2.5	1.3	1.9
131	2.3	1.1	2.0
139	2.3	0.9	2.5
141	2.4	1.1	2.1
155	0.7	0.2	3.2
157	0.5	0.13	3.8